*International Journal of Microwave and Wireless Technologies*

**cambridge.org/mrf**

# A PT-symmetric wireless power transfer system with dual-frequency switching capability

Wuji Sun, Na Kou and Shixing Yu

College of Big Data and Information Engineering, Guizhou University, Guiyang, People's Republic of China

**Research Paper**

**Cite this article:** Sun W, Kou N, Yu S (2026) A PT-symmetric wireless power transfer system with dual-frequency switching capability. *International Journal of Microwave and Wireless Technologies* **18**(1), 74–81. https://doi.org/10.1017/S1759078726103067

Received: 11 November 2025
Revised: 25 February 2026
Accepted: 4 March 2026

**Keywords:**
dual-frequency; parity-time; switch-mode amplifier; wireless power transfer

**Corresponding author:** Na Kou;
Email: nkou@gzu.edu.cn

**Abstract**

In this paper, a dual-frequency switchable wireless power transfer (WPT) system based on parity–time (PT) symmetry is proposed. For the transmitter, a high-efficiency switch-mode amplifier is employed as the negative impedance to provide the required gain. To realize dual-frequency operation, the magnetic coupling coil is designed as triple-tap structure which can be used to create two distinct series inductor-capacitor (LC) resonant branches by switch. At the receiver, two parallel inductor-capacitor-resistor (LCR) resonant circuits with corresponding dual operational frequency of transmitter are adopted to achieve stable energy reception. The transmission characteristics of the system under different frequency switching modes are analyzed theoretically and verified experimentally. The results demonstrate that, whether operating in the low- or high-frequency mode, the system can maintain the PT-symmetric state in the strong coupling regime, achieving robust and efficient WPT with system efficiency >80%. The proposed dual-frequency switchable WPT system can offer a theoretical reference for practical reconfigurable wireless charging applications requiring dual operating frequencies.

## Introduction

Wireless power transfer (WPT) has attracted increasing attention in recent years due to its promising applications in mobile electronics, biomedical implants, industrial sensors, and electric vehicles [1–4]. However, traditional resonant inductive coupling systems often suffer from performance degradation in the over-coupled regime, where mode (frequency) splitting occurs, and they are highly sensitive to environmental variations [5–7]. In conventional strongly coupled resonant WPT, frequency- or impedance-tuning strategies have been widely analyzed and experimentally validated using equivalent circuit models to cope with the frequency-splitting behavior in the over-coupled regime [8–10]. As a robust alternative, parity–time (PT) symmetric WPT architectures – conceptually derived from quantum mechanics [11] – have been introduced to balance internal gain and loss [12–14]. Since Assawaworrarit et al. first demonstrated that PT-symmetry enables stable energy delivery under strong coupling without active frequency tuning [15], subsequent research has extensively focused on improving efficiency and transmission range through advanced amplifiers, coil arrays, and optimized resonant topologies [16–19].

However, most PT-symmetric WPT systems operate at a single frequency, limiting their adaptability in scenarios with multiple device types, EMI, or dynamic resonant shifts [17, 20–22]. In practice, emerging applications increasingly demand systems that support multiple resonant frequencies or allow reconfiguration to meet diverse requirements [23–25]. Conventional approaches to realize multi-frequency operation typically rely on tap-switching or segmented-coil techniques [26–29]. While these methods can generate dual or multiple resonant modes, they usually require additional impedance matching or switching circuits and remain sensitive to coupling variation, thereby constraining robustness.

Motivated by these challenges, this work proposes a dual-frequency PT-symmetric WPT system that combines the adaptability of tap-switching with the robustness of PT symmetry. The proposed architecture provides two selectable PT operating points corresponding to two resonant modes, enabling dual-frequency operation without additional frequency-tracking control. We clarify the distinction between PT-symmetric self-oscillating gain–loss-balanced operation and conventional passive strongly coupled SP-compensated WPT, and validate the proposed design through theoretical modelling and experimental measurements demonstrating high efficiency in both modes.

© The Author(s), 2026. Published by Cambridge University Press in association with The European Microwave Association.

## System design

### Theoretical analysis

In a PT-symmetric WPT system, energy is injected into the source resonator through an active gain element and subsequently transferred to the load via resonant inductive coupling [19]. To achieve dual-frequency operation, the magnetic coupling component (inductor coil) can be tapped to connect with one more circuit branch, as shown in Fig. 1(a). This method can create two resonant modes for transmitter. In the proposed architecture, the transmitter incorporates two series-connected resonant branches corresponding to two distinct operating frequencies. To analyze the mode-dependent dynamics of the system, we introduce a binary frequency state variable $\sigma \in \{0,1\}$, where $\sigma = 0$ and $\sigma = 1$ denote the low- and high-frequency modes, respectively. And the switching index $\sigma$ represents the tapped-coil configuration, which changes the effective inductance. Besides, according to the framework of magnetic coupling resonance theory and to simplify the subsequent analysis, it is typically assumed that the transmitter and receiver share an identical self-resonant frequency. Under this condition, we employ a coupled-mode theory (CMT) formulation as a reduced-order approximation of the underlying compensated circuit model to capture the dominant near-resonant modal interaction and the gain–loss balance in the PT-symmetric WPT link [15]. The CMT model assumes near-resonant operation and slowly varying envelopes of the fundamental resonant modes; therefore, it does not explicitly account for switching harmonics, strong nonlinearities (e.g., device saturation), or distributed parasitics that may become relevant at higher power or far-from-resonance operation. With these assumptions, the mode-dependent dynamics of the coupled system can be expressed as follows:

$$\frac{\mathrm{d}}{\mathrm{d}t}\begin{bmatrix} a_s \\ a_r \end{bmatrix} = \begin{bmatrix} i\omega_1(\sigma) - g_n & -ik(\sigma) \\ -ik(\sigma) & i\omega_2(\sigma) + \varphi \end{bmatrix}\begin{bmatrix} a_s \\ a_r \end{bmatrix}. \quad (1)$$

where $k(\sigma)$ denotes the coupling coefficient under the selected frequency mode which can be given by

$$k(\sigma) = \begin{cases} k_L, & \text{if } \sigma = 0 \text{ (low - frequency mode)} \\ k_H, & \text{if } \sigma = 1 \text{ (high - frequency mode).} \end{cases} \quad (2)$$

The corresponding modal amplitudes are represented by $a_s$ and $a_r$, respectively. The net gain rate is expressed as $g_n = g - \varphi_s$, where $g$ denotes the overall gain provided by the negative resistance $R_N$, and $\varphi_s$ accounts for the inherent loss arising from the resistance of the transmitting coil. The total loss within the system is defined as $\varphi = \varphi_L + \varphi_r$, comprising both the load-induced dissipation $\varphi_L$ and the intrinsic ohmic loss of the receiving coil $\varphi_r$. Assuming the resonator amplitudes evolve proportionally as $e^{i\omega(\sigma)t}$. Besides, $\omega_1(\sigma)$ and $\omega_2(\sigma)$ denote the intrinsic (uncoupled) resonant angular frequencies of the source (Tx) and receiver (Rx) resonators under the switching state $\sigma$, respectively. To derive the characteristic equation, we assume the resonator amplitudes evolve proportionally as $a_s(t) = A_s\, e^{i\omega(\sigma)t}$, $a_r(t) = A_r\, e^{i\omega(\sigma)t}$, where $\omega(\sigma)$ is the steady-state oscillation angular frequency of the coupled system. Substituting these expressions into Eq. (1) and canceling the common factor $e^{i\omega(\sigma)t}$ yields the following algebraic equations:

$$\begin{aligned} [i(\omega(\sigma) - \omega_1(\sigma)) - g_n]A_s + ik(\sigma)A_r = 0 \\ ik(\sigma)A_s + [i(\omega(\sigma) - \omega_2(\sigma)) + \varphi]A_r = 0. \end{aligned} \quad (3)$$

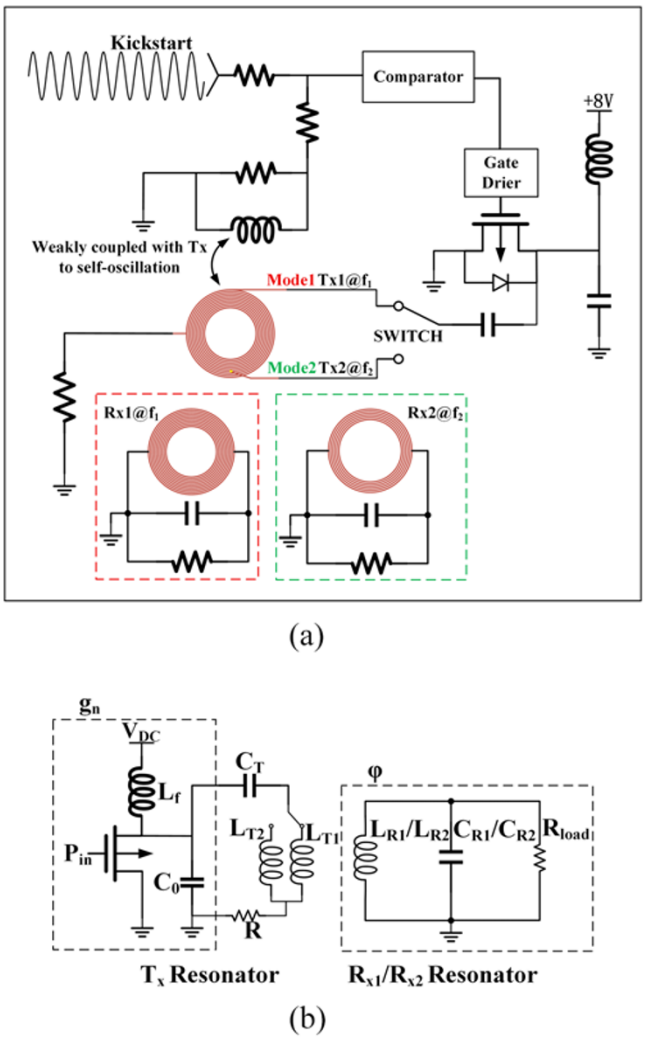



**Figure 1.** Schematic diagram of a switch-mode PT symmetric wireless power transfer circuit with dual-frequency switchability: (a) system configuration and (b) its equivalent circuit diagram.

These equations can be written in matrix form as

$$\begin{bmatrix} i(\omega(\sigma) - \omega_1(\sigma)) - g_n & ik(\sigma) \\ ik(\sigma) & i(\omega(\sigma) - \omega_2(\sigma)) + \varphi \end{bmatrix}\begin{bmatrix} A_s \\ A_r \end{bmatrix} = \begin{bmatrix} 0 \\ 0 \end{bmatrix}. \quad (4)$$

A non-trivial solution $(A_s, A_r) \neq (0, 0)$ exists only if the determinant of the coefficient matrix equals zero. Therefore, the characteristic equation is obtained as

$$(\omega(\sigma) - \omega_1(\sigma) + ig_n)(\omega(\sigma) - \omega_2(\sigma) - i\varphi) - k(\sigma)^2 = 0. \quad (5)$$

To determine the eigenfrequencies of the system, we solve the characteristic Eq. (5) and obtain

$$(\omega(\sigma) - \omega_1(\sigma))(\omega(\sigma) - \omega_2(\sigma)) + g_n\varphi - k(\sigma)^2 = 0. \quad (6)$$

$$\varphi(\omega(\sigma) - \omega_1(\sigma)) - g_n(\omega(\sigma) - \omega_2(\sigma)) = 0. \quad (7)$$

From Eqs. (6) and (7), set the real and imaginary parts to zero, respectively, and assuming that $\omega_2(\sigma) = \omega_1(\sigma) = \omega_0(\sigma)$, where

https://doi.org/10.1017/S1759078726103067 Published online by Cambridge University Press

$\omega_0(\sigma)$ denotes the common uncoupled resonant angular frequency of the Tx/Rx resonators under the switching state σ, thus we can calculate the eigenfrequency $\omega(\sigma)$ as

$$\omega(\sigma) = \begin{cases} \omega_0(\sigma) \pm \sqrt{k^2(\sigma) - \varphi^2}, & k(\sigma) \geqslant \varphi \\ \omega_0(\sigma), & k(\sigma) < \varphi. \end{cases} \tag{8}$$

$\omega_0(\sigma)$ can be expressed as

$$\omega_0(\sigma) = (1-\sigma)\omega_L + \sigma\omega_H. \tag{9}$$

The Eq. (8) reveals two distinct dynamic regimes depending on the relative magnitude of $k(\sigma)$ and the total system loss $\varphi$.

In the strong coupling regime in which $k(\sigma) > \varphi$, the square root term in Eq. (8) is real, and the system supports two distinct real eigenfrequencies symmetrically split around $\omega_0(\sigma)$. This corresponds to the unbroken PT-symmetric phase, in which the system sustains stable oscillation at either of the two eigenmodes with balanced energy exchange between gain and loss. The frequency splitting also increases with stronger coupling, reflecting enhanced mode hybridization.

In contrast, in the weak coupling regime where $k(\sigma) < \varphi$, the square root becomes imaginary, resulting in a pair of complex conjugate eigenfrequencies. This indicates the system is in the broken PT-symmetric phase, where the modal amplitudes become exponentially growing or decaying, and the system effectively operates at a single dominant resonance near $\omega_0(\sigma)$.

By inserting the respective frequency solutions corresponding to these two regimes into the coupled dynamic equations, one can extract distinct transmission behaviors that signify the system's symmetry state.

Following the coupled-mode power-balance formulation in Assawaworrarit and Fan (Nature Electronics, 2020), the load is modelled as an additional dissipative channel of the receiver resonator characterized by the load-induced loss rate $\varphi_L$. With the same CMT energy normalization, the time-averaged power extracted by a dissipative channel is proportional to the corresponding loss rate and the steady-state energy stored in that resonator mode (see Supplementary Eqs. (S1.6)–(S1.7) in [15]). Therefore, the delivered load power $P_{load}$ can be written in the closed form given in Eq. (10). For each receiver resonator, the power delivered $P_{load}$ and the transmission efficiency $\eta$ can be written as

$$P_{load} = \omega_0(\sigma)\varphi|a_s|^2 = \begin{cases} \frac{\omega_0(\sigma)k(\sigma)^2}{\varphi}|a_s|^2, & k(\sigma) < \varphi \\ \omega_0(\sigma)\varphi|a_s|^2, & k(\sigma) \geqslant \varphi. \end{cases} \tag{10}$$

$$\eta = \frac{\varphi_l|a_r|^2}{\varphi_s|a_s|^2 + (\varphi_r+\varphi_l)|a_r|^2} = \begin{cases} \frac{1-\frac{\varphi_r}{\varphi_r+\varphi_l}}{1+\frac{\varphi_s}{\varphi_r+\varphi_l}}, & k(\sigma) \geqslant \varphi \\ \frac{1-\frac{\varphi_r}{\varphi_r+\varphi_l}}{1+\frac{\varphi_s(\varphi_r+\varphi_l)}{k(\sigma)^2}}, & k(\sigma) < \varphi. \end{cases} \tag{11}$$

The transfer efficiency is defined as $\eta = P_{load}/P_{in}$. Following the power-balance derivation in the Supplementary Information of [15], the injected power is distributed among the intrinsic loss of the Tx resonator, the intrinsic loss of the Rx resonator, and the load dissipation (modelled by $\varphi_L$). With the same CMT energy normalization, substituting the steady-state modal amplitudes of the coupled system into this power-balance relation yields the analytical efficiency expression reported in Eq. (11).

From Eqs. 10 and 11, it can be observed that when $k \geq \varphi$, the power delivered to the load and the transmission efficiency of the system both become independent of the coupling coefficient. Besides, when $k < \varphi$, the transmission efficiency is primarily determined by the intrinsic loss at the source side $\varphi_s$ and the total loss at the receiver side $\varphi$. Moreover, since $\varphi_s \ll \varphi$, the system is capable of sustaining highly efficient energy transfer.

**Table 1.** Parameters of the circuit

| Components | Value | Unit |
|---|---|---|
| $L_f$ | 150 | μH |
| $C_T$ | 3.2 | nF |
| $C_0$ | 6.7 | nF |
| $C_{R1}$ | 3 | nF |
| $C_{R2}$ | 1.65 | nF |
| $R_{load}$ | 870 | Ω |

### *Architecture*

As shown in Fig. 1(a), the negative-resistance source is realized by an *N*-channel MOSFET (IRF840, TO-220 package) operated in the switch-mode. The IRF840 is chosen for its high breakdown voltage (500 V) and adequate switching speed (turn-on delay 25–60 ns, rise time 75–160 ns), which are sufficient for the 400–800 kHz operating range. To generate the gate signal, a 5 V sinusoidal waveform from a function generator is first converted into a square waveform using a high-speed comparator (LT1711, Analog Devices). This square wave is then buffered by a gate driver (LM5114, Texas Instruments), which provides large source/sink current capability to rapidly charge and discharge the input capacitance ($C_{iss} \approx 1300$ pF) of the IRF840, thereby ensuring sharp switching transitions. The amplifier is powered by a regulated 8 V DC supply, corresponding to a maximum experimental input power of approximately 2 W. Once oscillation is initiated, the circuit maintains self-sustained operation without external feedback control, leveraging the intrinsic nonlinear behavior of the MOSFET stage to satisfy the PT-symmetry condition.

To ensure efficient power delivery, the impedance matching network of the proposed system is realized by the series–parallel (SP) resonant topology shown in Fig. 1(b). Specifically, the capacitor $C_0$ is connected in shunt with the switching transistor to provide voltage shaping and soft switching conditions, while the series branch composed of $C_T$ and the transmitting coil inductance $L_T(\sigma)$ compensates the equivalent input reactance at both resonant modes (i.e., $L_T(\sigma = 1) = L_{T1}$ and $L_T(\sigma = 2) = L_{T2}$). In this way, the effective input resistance seen from the MOSFET drain is maintained close to zero at resonance, thereby satisfying the PT-symmetric condition while simultaneously maximizing power transfer. Additionally, the load is modeled as an equivalent resistance *R*, which represents the reflected impedance of the receiving coil together with its rectified load.

In addition, the parameters of other components in the circuit are shown in Table 1. In the proposed system, to enable dual-frequency operation within a compact and efficient WPT architecture, a tapped transmitting coil was developed using a single-layer planar winding structure. The coil is fabricated with 0.05 mm × 1000-strand Litz wire to reduce AC resistance and minimize skin and proximity losses, ensuring high Q-factor performance. As illustrated in Fig. 2, a total of 16 turns is wound on a planar frame. A tapped point is introduced at the 10th turn

https://doi.org/10.1017/S1759078726103067 Published online by Cambridge University Press

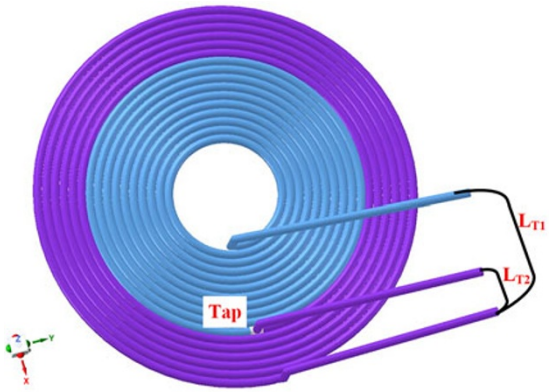



**Figure 2.** Model of the transmitting coil.

(counted from the inner end), at this tapping location, the enamel insulation is locally removed by chemical stripping combined with thermal treatment, ensuring that the copper strands are cleanly exposed without mechanical damage. The exposed strands are then consolidated and soldered using medium-temperature solder paste with a controlled hot-air process, followed by precision reinforcement with a soldering iron to provide mechanical stability. To minimize parasitic effects, the tapping lead is kept as short as possible and aligned with the winding plane, which reduces additional inductance and contact resistance. This fabrication approach yields a stable low-resistance connection while preserving the high-Q characteristics of the transmitting coil.

The coil is thus divided into two effective segments: one is from the tapping point to the outermost turn which corresponds to $L_{T1}$, and the other is from the innermost turn to the outermost turn, corresponding to $L_{T2}$. To enable dynamic frequency reconfigurability, the transmitter incorporates a switch, which is used to select between these two resonance modes. When the switch enables the full coil path, the system operates in low-frequency mode; otherwise, it operates using only the outer segment for high-frequency mode. This tapped structure avoids the need for two separate coils or bulky relay switching, effectively reducing PCB area, parasitic couplings, and circuit complexity.

## Experimental setup and results

### Experimental setup

To ensure proper resonance and PT symmetry in both modes, two receiver branches are designed, each equipped with a resonant coil as shown in Fig. 3(b) and a set of matching components, including a compensation capacitor and resistor, selected to align the resonant frequency and balance the overall loss.

The detailed geometric and electrical parameters of the transmitting and receiving coils are summarized in Table 2.

Figure 4 shows the experimental setup of the proposed WPT system. A DC power supply is used to power the comparator, gate driver, and MOSFET-based switching units, while a function generator is employed to provide an initial excitation signal to assist the startup of the self-oscillating circuit. The oscilloscope is used to monitor the voltage waveforms at both the transmitter and receiver ends.

### Measurement procedure

Based on the dual-frequency architecture, two operating modes are tested under low-frequency and high-frequency conditions. For this first prototype, the delivered power is intentionally kept at a modest level for experimental safety and reliable proof-of-concept validation, because the switch-mode negative-resistance stage together with the resonant network may generate relatively high RF voltage/current stress during self-oscillation. The voltage waveforms at both the transmitter and receiver ends are monitored and recorded to evaluate the system efficiency and delivered load power. To ensure reproducibility, the delivered load power and end-to-end efficiency are evaluated from directly measured RMS/DC quantities after the circuit reaches steady state at each transfer distance. The DC input power is obtained from the laboratory DC power supply as $P_{in} = V_{DC}\, I_{DC}$, where $V_{DC}$ and $I_{DC}$ are directly read from the DC supply display. On the receiver side, the steady-state RMS voltage $V_{RMS}$ is measured by the oscilloscope across the receiver LC branch (i.e., the voltage across the parallel resonant tank). The delivered load power is calculated as $P_{load} = V^2_{rms}/R_{load}$ and the end-to-end efficiency is computed as $\eta = P_{load}/P_{in}$. Here, $R_{load}$ denotes the effective load resistance under steady-state operation. In practice, it is obtained by combining the physical load resistor with the non-ideal receiver LC branch at the peak of the parallel-resonance curve (accounting for parasitics such as coil AC resistance and capacitor ESR). All RMS values are recorded after the output waveform becomes periodic and the operating frequency is stabilized for each distance.

### Measurement results

Figure 5(a) shows the calculated and measured eigenfrequencies of low-frequency operating WPT system, which indicates that the operating frequency split into two distinct branches ranging from approximately 280 to 510 kHz when the transmission distance $D_1$ between Tx and Rx1 is less than 65 mm indicating strong coupling

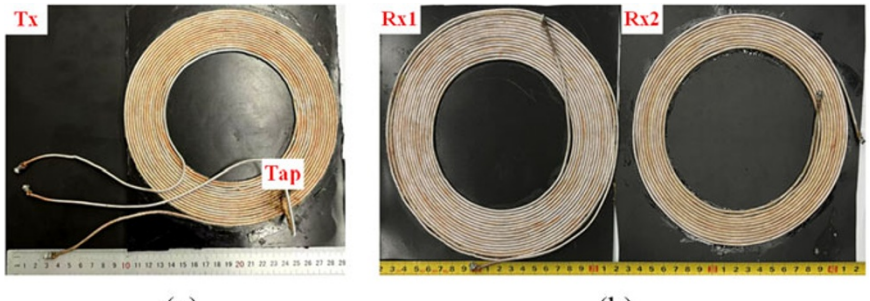



**Figure 3.** Structure of Tx and Rx coils: (a) Tx coil and (b) Rx coils.

https://doi.org/10.1017/S1759078726103067 Published online by Cambridge University Press

**Table 2.** The detailed geometric and parameters of the transmitting and receiving coils

| Coil | Dimensions (mm) ($Wi \times Wo \times H$) | Inductance (μH) | Number of Turns |
|---|---|---|---|
| $L_{T1}$ | 120 × 195 × 2 | 49.8 | 15 |
| $L_{T2}$ | 165 × 195 × 2 | 23.9 | 6 |
| $L_{R1}$ | 120 × 190 × 2 | 23.8 | 14 |
| $L_{R2}$ | 130 × 175 × 2 | 50.1 | 9 |

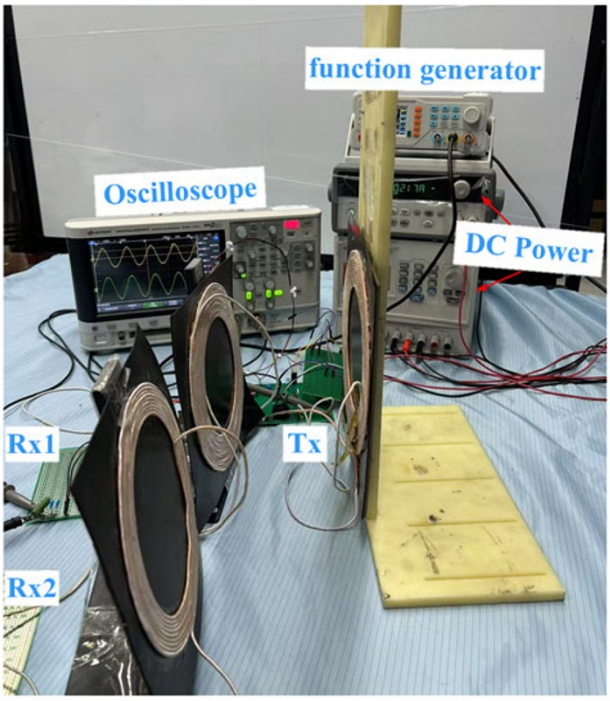



**Figure 4.** Experimental implementation of the proposed dual-frequency PT-symmetric WPT system.

region. As $D_1$ increases, the operational frequency converges to 398 kHz, presenting a transition into the weak coupling region. The corresponding system efficiency $\eta$ and delivered power $P_{load}$ are depicted in Fig. 5(b), illustrating that the measured $\eta$ remains above 80% in the strongly coupled region, and gradually decreases as $D_1$ increases. The measured delivered power at the load maintains approximately 1.0 W when $D_1 \leq 60$ mm and drops to 0.2 W as $D_1$ equals to 120 mm.

For the high-frequency mode of proposed WPT system, the operational frequency, system efficiency and delivered power level are shown in Figs. 6(a)–(b). It shows a wider frequency split range from 630 to 960 kHz than that under the low-frequency mode when the transmission distance $D_2 \leq 60$ mm., after which the system enters the weak coupling region. The measured frequency aligns well with the lower branch of calculated one, which stabilizes at 801 kHz beyond the bifurcation point. Figure 6(b) illustrates that the measured system efficiency remains above 80% within 60 mm, and decreases as $D_2$ gets longer. The delivered power at strong coupling area can reach 1.95 W and maintains values above 1.0 W when $D_2 = 95$ mm. Even at 100 mm, the power remains at about 0.9 W.

From analyses above, the strong coupling region in the high-frequency mode is approximately 5 mm shorter than that in the low-frequency mode, due to the more rapid spatial decay of the electromagnetic field at higher frequencies. However, the delivered power is nearly doubled compared to the low-frequency case. This enhancement can be attributed to higher voltage swing and improved power conversion efficiency of the switching amplifier under high-frequency. Moreover, the receiver branch designed for the high-frequency mode may exhibit better impedance matching, enabling more efficient power absorption. These results highlight the dual-frequency WPT system's ability to adaptively optimize power delivery across different operating modes.

### *Comparison and discussion*

Such a dual-frequency switching mechanism enhances the system's versatility and makes it more suitable for application scenarios requiring adaptive power delivery under varying frequencies or load conditions.

In comparison with prior studies in Table 3, conventional tapped-coil WPT systems [30] and dual-band designs using reactance-steering networks with reconfigurable receivers [31] demonstrate multi-frequency operation but suffer from efficiency degradation and strong dependence on coupling, with reported efficiencies often falling below 75%. On the other hand, PT-symmetric WPT schemes [32] maintain robust efficiency under varying distances but are limited to single-frequency operation. By combining both advantages, the proposed PT-symmetric dual-frequency architecture achieves stable efficiency above 80% in both operating modes, offering both frequency flexibility and coupling robustness. This dual contribution positions the system as a promising candidate for future adaptive and reliable WPT applications.

In addition to these performance advantages, practical deployment also requires considerations on power scaling and loading conditions. For this first prototype, the delivered power was intentionally kept at a modest level for experimental safety and reliable proof-of-concept validation, because the switch-mode negative-resistance stage and resonant network may produce high RF voltage/current stress during self-oscillation. For higher-power applications, scaling the delivered power requires co-optimization of the resonant link and the power stage, e.g., improving the coupling/coil quality factor (higher $k$ and $Q$) and selecting low-loss switching devices and passive components with sufficient voltage/current and thermal margins, while maintaining oscillator stability and EMI compliance.

Another practical consideration is multi-receiver operation. In multi-receiver scenarios, the transmitter generally sees an effective load that depends on the number of receivers and their operating states due to the reflected impedance from each receiver. As a result, the effective load-induced loss (e.g., an equivalent $\varphi_L$ term in the coupled-mode formulation) is no longer constant and may vary with receiver connection/disconnection and load changes. Such variations can shift the steady operating point and consequently affect the PT gain–loss balance condition as well as the coupling threshold separating different operating regimes (e.g., the onset of frequency splitting). Therefore, although the proposed dual-frequency architecture (tapped-coil switching at the transmitter together with receiver matching networks) provides a convenient front-end that may be extendable to multi-receiver applications, a complete multi-receiver model and its validation are beyond the scope of this work and will be investigated in future studies.

https://doi.org/10.1017/S1759078726103067 Published online by Cambridge University Press

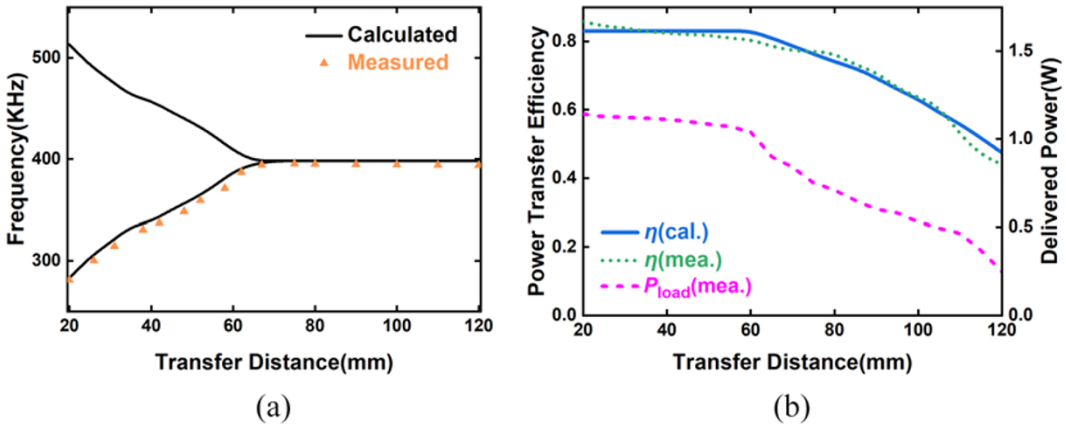



**Figure 5.** System frequency and power transfer characteristics under low-frequency mode: (a) eigenfrequency vs. transfer distance; (b) efficiency and delivered power vs. distance.

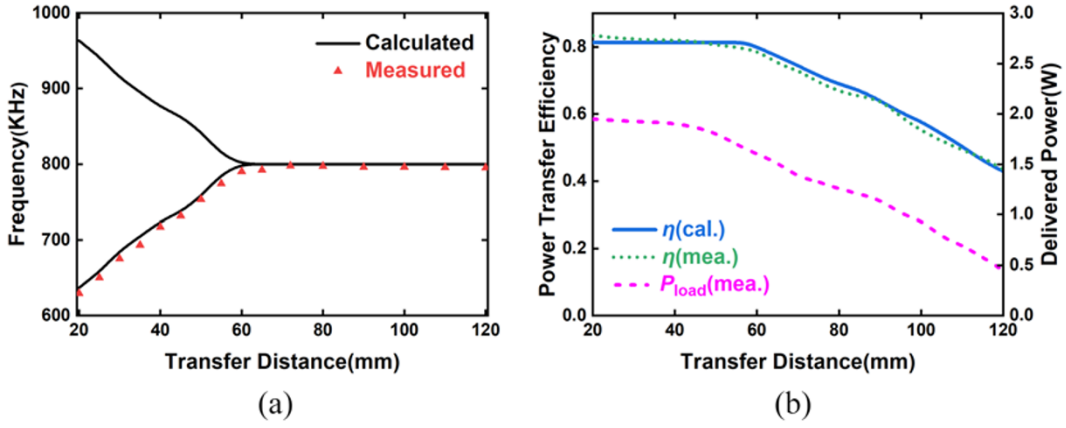



**Figure 6.** System frequency and power transfer characteristics under high-frequency mode: (a) eigenfrequency vs. transfer distance; (b) efficiency and delivered power vs. distance.

**Table 3.** Performance Comparison

| Reference | Method | PT symmetry | Multi-frequency | Efficiency/performance |
|---|---|---|---|---|
| [30] | Zone-impedance matching with tapped TX coil for long-distance WPT | No | No | Efficiency decreases significantly with distance (drops to ~60% at long range) |
| [31] | Reactance steering network with reconfigurable receivers (dual-band at 100 kHz & 13.56 MHz) | No | Yes | 82.5% @ 100 kHz; 74.8% @ 13.56 MHz (2.8 cm distance) |
| [32] | PT-symmetric WPT for range extension | Yes | No | Maintains >70% efficiency at 40 cm (≈72%), vs. <50% conventional |
| This work | PT-symmetric WPT with tapped-coil dual-frequency switching | Yes | Yes | >80% efficiency in both modes, stable across strong coupling |

## Conclusion

In this work, we investigate a dual-frequency switchable WPT system based on PT symmetry. Both theoretical analysis and experimental results verify that the proposed system maintains efficient and robust power transfer at two resonant operating frequencies. By controlling the on/off states of two LC resonant branches, the transmitter can switch between two distinct operating modes while preserving the PT-symmetric steady state. The proposed architecture provides a practical reference for reconfigurable dual-frequency WPT operation under varying coupling conditions. Future work will consider power scaling and extension to more complex loading conditions (e.g., multi-receiver operation) with dedicated modelling and validation.

**Acknowledgment.** This work was supported in part by the National Natural Science Foundation of China under Grant (62261007, 62361008) and in part by the Guizhou Provincial Basic Research Program (Natural Science) under Grant QKHJC MS [2025] 594.

**Competing interests.** The authors declare that they have no known competing financial interests or personal relationships that could have appeared to influence the work reported in this paper.

https://doi.org/10.1017/S1759078726103067 Published online by Cambridge University Press

## References


1. **Lu C, Huang X and Liu M** (2021) Investigation of wireless power transfer with non-perfect planar metamaterial. *AEU – International Journal of Electronics and Communications* **137**, 153783.
2. **de Miranda CM, Oliveira AB and Freire RCS** (2022) A three-coil wireless power transfer system using self-resonant coils. *AEU – International Journal of Electronics and Communications* **148**, 154281.
3. **Wang J, Zhang L and Chen Y** (2023) A combinable wireless power transfer design for extensible-capacity and adaptive charging of route UAVs. *AEU – International Journal of Electronics and Communications* **165**, 154559.
4. **Moeini S, Horestani AK and Fumeaux C** (2023) Microwave wireless power transfer system using a dual-dielectric resonator. *AEU – International Journal of Electronics and Communications* **170**, 154668. https://doi.org/10.1016/j.aeue.2023.154836.
5. **Yang K, Yu S and Kou N** (2024) Wireless power transfer system with multi conformal receivers based on PT symmetry. *AEU – International Journal of Electronics and Communications* **180**, 154832.
6. **Xie J, Chen Y, Zhou Y and Luo C** (2025) A compact dual-channel WPT system based on decoupled integrated coils for power enhancement. *IEEE Transactions on Circuits and Systems Part II: Express Briefs* **72**(9), 1243–1247.
7. **Lee Y-S, Yoon T, Song YJ, Hong SK, Oh J and Nam S** (2025) Transmission-conversion efficiency maximization technique for MIMO wireless power transfer systems in ISAC applications. *IEEE Antennas and Wireless Propagation Letters* **24**(11), 4492–4496. https://doi.org/10.1109/LAWP.2025.3578089.
8. **Heebl JD, Thomas EM, Penno RP and Grbic A** (2014) Comprehensive analysis and measurement of frequency-tuned and impedance-tuned wireless non-radiative power-transfer systems. *IEEE Antennas and Propagation Magazine* **56**(4), 44–60. https://doi.org/10.1109/MAP.2014.6931657
9. **Liu D, Hu H and Georgakopoulos SV** (2016) Misalignment sensitivity of strongly coupled wireless power transfer systems. *IEEE Transactions on Power Electronics*. https://doi.org/10.1109/TPEL.2016.2605698
10. **Sis SA and Kavut S** (2018) A frequency-tuned magnetic resonance-based wireless power transfer system with near-constant efficiency up to 24 cm distance. *Turkish Journal of Electrical Engineering and Computer Sciences* **26**(6), 3168–3180. https://doi.org/10.3906/elk-1803-98
11. **Stolz K and Müller R** (2018) Magnetically coupled resonance WPT: Review of compensation topologies and frequency splitting. *Electronics* **7**(11), 296. https://doi.org/10.3390/electronics7110296.
12. **Dai Z, Peng W, Wang Z, Li M, Zhou Y, Wang R, Chen T, Zhang X and Wang J** (2024) Reconfigurable receiver with adaptive output voltage for wireless power transfer. *IEEE Transactions on Circuits and Systems I: Regular Papers* **71**(1), 454–462.
13. **Li X, Chen Y and Wang Z** (2022) Frequency splitting suppression in wireless power transfer using hemispherical spiral coils. *AIP Advances* **12**(5), 055016. https://doi.org/10.1063/5.0078744.
14. **Sun C, Yang W, He Y, Dong C, Liang X, Wei Y, Chen H and Sun NX**(2021) Electrostatically tunable mutual inductance for frequency splitting elimination in wireless power transfer. *IEEE Transactions on Magnetics* **58**(99), 1–1.
15. **Assawaworrarit S and Fan S** (2020) Robust and efficient wireless power transfer using a switch-mode implementation of a nonlinear parity-time symmetric circuit. *Nature Electronics* **3**(5), 273–279. https://doi.org/10.1038/s41928-020-0399-7.
16. **Yan X and Yan W** (2024) Analysis of the parity-time symmetry model in the receiver-based wireless power transfer. *Energies* **17**(23), 6103. https://doi.org/10.3390/en17236103.
17. **Pham CD, Ha-Van N, Le MT, Nguyen K and Sekiya H** (2025) Comparative experiment of conventional and dynamic theories for wireless power transfer. *IEEE Microwave and Wireless Technology Letters* **35**(9), 1428–1431. https://doi.org/10.1109/LMWT.2025.3568399.
18. **Özdemir ŞK, Rotter S, Nori F and Yang L** (2019) Parity-time symmetry and exceptional points in photonics. *Nature Materials* **18**, 783–798. https://doi.org/10.1038/s41563-019-0304-9.
19. **Assawaworrarit S, Yu X and Fan S** (2017) Robust wireless power transfer using a nonlinear parity–time-symmetric circuit. *Nature* **546**, 387–390. https://doi.org/10.1038/nature22404.
20. **Zhang Z, Chen Z and Cao Y** (2025) 6.78 MHz double transmitting coils classe2wireless power transfer system based on PT symmetry. *International Journal of Circuit Theory and Applications* **53**(11), 6162–6174.
21. **Chen YH, Qiu DY, Rong C, Zhang B and Shu XJ** (2023) A double transmitting coil wireless power transfer system based on parity time symmetry principle. *IEEE Transactions on Power Electronics* **39**, 3289–3299. https://doi.org/10.1109/tpel.2023.3338109.
22. **Zhang H, Zhu K, Guo Z, Chen Y, Sun Y, Jiang J, Li Y, Yu Z and Chen H** (2023) Robustness of wireless power transfer systems with parity-time symmetry and asymmetry. *Energies* **16**(12), 4605. https://doi.org/10.3390/en16124605
23. **Atallah HA, Hussein R and Abdel-Rahman AB** (2022) Tunable Dual-Band Wireless Power Transfer (TDB-WPT) system for short range applications. *IEEE Transactions on Circuits and Systems Part II: Express Briefs* **70**(99), 1–1.
24. **Hong W, Wang J, Lim EG, Leach M, Wang Z, Pei R and Huang Y** (2025) Compact distance-adaptive wireless power transfer using a reconfigurable auxiliary coil. *IEEE Antennas and Wireless Propagation Letters* **24**, 1–5. https://doi.org/10.1109/LAWP.2025.3526916
25. **Mercier PP and Chandrakasan AP** (2013) Rapid wireless capacitor charging using a multi-tapped inductively-coupled secondary coil. *IEEE Transactions on Circuits and Systems I: Regular Papers* **60**(9), 2263–2272. https://doi.org/10.1109/TCSI.2013.2246231.
26. **Jabbar A, Rehman MA, Javed A, Awan MS and Iqbal J** (2023) Efficient compact radiative near-field wireless power transfer to miniature biomedical implants. *IEEE Antennas and Wireless Propagation Letters* **22**(12), 2803–2807. https://doi.org/10.1109/LAWP.2023.3298350.
27. **Yin Z, Yu S and Kou N** (2024) Robust wireless power transfer system using gain element as source for conformal application. *IEEE Microwave and Wireless Technology Letters* **34**(1), 127–130. https://doi.org/10.1109/LMWT.2023.3336000
28. **Ding C, Feng L, Wu P, Wang G and Cheng Y** (2025) Generalized PT-symmetric wireless power transfer systems with laterally arranged multirelays. *IEEE Microwave and Wireless Technology Letters* **35**(3), 366–369. https://doi.org/10.1109/LMWT.2025.3526140.
29. **Seo S** (2024) A hybrid transmitting coil for improving angular freedom of a wireless power transfer system. *IEEE Microwave and Wireless Technology Letters* **34**(1), 1–4.
30. **Hu J, He L, Liu H, Ng RWM and Lee C-K** (2022) Using zone impedance matching technique to improve the power transfer capability of an inductive charging system over a long distance. *Electronics* **11**(13), 1982. https://doi.org/10.3390/electronics11131982.
31. **Liu M and Chen M** (2019) Dual-band wireless power transfer with reactance steering network and reconfigurable receivers. In Proceedings IEEE Applied Power Electronics Conference and Exposition. (APEC), Anaheim, CA, USA, pp. 1418–1423.
32. **Qu Y, Zhang B, Gu W, Li J and Shu X** (2023) Distance extension of S-PS wireless power transfer system based on parity-time symmetry. *IEEE Transactions on Circuits and Systems Part II: Express Briefs* **70**(8), 2954–2958.


https://doi.org/10.1017/S1759078726103067 Published online by Cambridge University Press



**Wuji Sun** received his Bachelor of Science degree in Electronic Information Engineering from Ludong University in 2022. Currently, he is pursuing his Master's degree at the Ministry of Education's Engineering Research Center for Power Semiconductor Device Reliability, School of Big Data and Information Engineering, Guizhou University. His main research area is wireless power transmission.



**Shixing Yu** received a bachelor's degree in Electronic Information Engineering from the School of Electronic Engineering, Xidian University, China in 2012. He obtained a Ph.D. degree in Electromagnetic Fields and Microwave Technology from the same school at Xidian University, China in 2017. Currently, he holds the position of Associate Professor at the College of Big Data and Information Engineering, Guizhou University, China. He has authored more than 30 research articles and his current research interests include antenna and array, electromagnetic field theory, artificial electromagnetic structures, microwave devices, radio-frequency circuits, and microwave measurement.



**Na Kou** received a bachelor's degree in Electronic Information Engineering from the School of Electronic Engineering, Xidian University, China in 2013. He obtained a Ph.D. degree in Electromagnetic Fields and Microwave Technology from the same school at Xidian University, China in 2018. Currently, she holds the position of Associate Professor at the College of Big Data and Information Engineering, Guizhou University, China. She has authored more than 20 research articles and her current research interests include array antennas, conformal antennas, frequency-selective radar absorbers, wireless power transfer, and vortex electromagnetic fields.

https://doi.org/10.1017/S1759078726103067 Published online by Cambridge University Press